Research and application of macro-micro fracture correlation of heterogeneous granite

Yunjuan Chen[1,2], Jiarui Su[2]*, Tao Gao[3], Yi Jing[4], Huifu Zhang[2], Hongjie Duan[2] and Wenbin Zhao[2]

[1]Key Laboratory of Building Structural Retrofitting and Underground Space Engineering, Ministry of Education, Shandong Jianzhu University, Jinan, China, [2]Civil Engineering College, Shandong Jianzhu University, Jinan, China, [3]Shandong Earthquake Agency, Jinan, China, [4]School of Qilu Transportation, Shandong University, Jinan, Shandong, China

Granite structure has the characteristics of discrete distribution and random distribution of minerals, which is particularly critical to the stability of surrounding rock of underground caverns, and the research process is extremely complicated. In this paper, the granite of Dagangshan tunnel in rock sections of class III was taken as the research object, and the mineral composition and proportion, the macro and micro characteristics of granite was analyzed by XRD analysis, SEM and laboratory compressive test; Dagangshan tunnel's section model with surrounding rock of class III was established using the particle flow program PFC and the numerical simulation was done, thus the influence of micro composition and proportion on surrounding rock masses' stability with the tunnel excavation was analyzed. Results show that: The content of illite and albite is the most, and illite is the weak mineral of the granite. For the granite of Dagangshan tunnel with rock masses of class III, the rock failure is mainly caused by shear force and secondary by tensile force. Fracture is mainly concentrated in the enrichment area of "weakened minerals," where as the breakthrough point and expands to other parts, and further connects. The "enhanced minerals" are basically stable because of their high hardness and strong link between each other. After tunnel excavation, cracks of tunnel's side walls and the arch foots are more serious, so the supporting measures of these parts should be strengthened.

KEYWORDS

heterogeneous, granite, test, numerical simulation, macro-micro scopic correlation

1 Introduction

Heterogeneous granite has multi-scale characteristics, and its mechanical properties have spatial variation. The rupture correlation is affected by many factors (Shi et al., 2020; Xu et al., 2020; Huang et al., 2021a; Vahid and Abbas, 2021; Li et al., 2023; Chen et al., 2022a), which not only affects the stability of surrounding rock of underground caverns, but also increases the difficulty of stability evaluation. By studying the macroscopic and microscopic fracture of granite and establishing the correlation between the microscopic structure of rock mass and macroscopic fracture, we can deeply understand the mechanism and process of rock fracture, which is of great significance for the safe construction and green operation of engineering construction. At the same time, it can also provide important support for predicting and controlling the fracture behavior of rock (Xia et al., 2021; Chen et al., 2022b; Chen et al., 2022c; Sun et al., 2019; Han et al., 2023).

In recent years, both domestic and international scholars have conducted experimental and simulation studies on the macro-micro failure characteristics of rock mass and rock heterogeneity (Peng and Chen, 2021; Liu et al., 2020; Zhang et al., 2022). Based on the macro-micro structure of layered rock mass, Liu et al. (2021) derived an anisotropic multi-scale damage model and permeability evolution equation for saturated layered rock mass under hydraulic coupling load within the framework of thermodynamics. Zheng et al. (2005) carried out meso-CT scanning test on fractured rock, and found that the damage evolution and crack propagation of rock were affected by different minerals in the rock. Cracking and failure generally began from the surface with weak mineral strength. Through uniaxial compression simulation, Ni et al. (2015) found that particle size is an important factor affecting rock mass fracture. Voronoi diagram is introduced to analyze elastic modulus and flexibility. It is found that elastic modulus is inversely proportional to size, and flexibility does not change significantly with rock mass size. Zhang et al. (2017) investigated the micro-level damage process of rock mass using PFC3D particle flow program and obtained its evolutionary law. Yang (2018), based on experimental research and numerical simulation, compared contact force chains and velocity fields in the micro structure of rock mass, suggesting that changes in the micro field are essentially consistent with macro state evolution. Li, (2017) established a three-dimensional inhomogeneity rock model by RFPA numerical simulation software, and believed that the damage evolution of rock and the internal meso-inhomogeneity have a direct impact, and pointed out that the meso-mineral composition of rock materials is the essential reason that affects the macro-strength and fracture mode. Yang et al. (2016) concluded based on discontinuous deformation (DDA) simulation platform that macro strength of rock masses is closely related to their micro non-uniformity. Huang et al. (2021b) established a 3D DFN numerical model to investigate seepage characteristics of fractured rocks, and found out mineral composition, distribution as well as fracture grid had significant impacts.

Li (2017) found that the uneven mineral composition of rock samples has a direct effect on the degree of fragmentation of rock failure by using PFC particle flow method and random analysis method simulation. At the same time, it also proves the accuracy of using discrete element method to simulate the non-uniform characteristics of rock. Liu et al. (2019) carried out the Brazilian disc acoustic emission test of granite and marble, and combined with scanning electron microscopy to analyze the microscopic morphology of the fracture surface. It was found that the macroscopic and mesoscopic crack propagation and failure of rock were mainly affected by the properties of weak mineral particles.

Most of the existing studies have primarily focused on analyzing the macro and micro fracture characteristics of granite, without exploring the macro-micro correlation. To address this gap, this study investigates the macro-micro failure characteristics of rock, as well as the type and composition ratio of mineral particles in III-level surrounding rock section of Dagangshan Tunnel. This is achieved through XRD testing, SEM analysis, and uniaxial compression tests conducted on granite specimens collected from the site. Subsequently, a numerical calculation model for non-uniform granite with particle flow is established to compare the influence of different types of mineral particles on surrounding rock stability.

2 Project overview

The Dagangshan Tunnel of Luding-Asbestos Expressway is situated in the southeastern periphery of the Tibetan Plateau, with its planned route extending from the Sichuan Basin to the central region of southwest high mountains in Sichuan. This area is characterized by towering mountains, frequent geological movements, extensive and deep valleys, as well as numerous glacial activities within the Dadu River basin water system. Groundwater primarily occurs in shallow weathering fissures, tectonic fissures, and deep tectonic fissures on slopes. The water content within these fissures is abundant, resulting in generally favorable hydrological conditions throughout this region. The overall topography exhibits a ladder-like pattern with elevated peaks towards the west gradually descending towards lower elevations in the east. Spanning a total length of 7,254 m, this tunnel represents an exceptional engineering feat due to its considerable length. The slope of the tunnel entrance and exit ranges from 25° to 30°, and the tunnel is extensively distributed within the granite geological layer. Due to the influence of engineering geological characteristics, the initial support in the study section consists of C25 concrete sprayed with a thickness of 22 cm, allowing for an anticipated deformation of up to 8 cm. The secondary lining comprises a waterproof C30 concrete with a thickness of 35 cm. This study focuses on Section K57+960~K58+060, which represents a III-level surrounding rock condition. Figure 1 illustrates the geological profile and sampling point locations within the tunnel. The granite in this section consists mainly of weathered granite, a relatively hard rock with a massive structure. The overall rock mass is relatively intact, with localized joints and fractures present. Groundwater primarily occurs through dripping, rainfall, and small streams. The elevation at the tunnel is situated at 1,214°m, while reaching an elevation peak at 2,114 m above sea level for mountain topography; consequently resulting in a burial depth of approximately 900 m.

3 Fracture laws analysis for granite of laboratory-scale

In order to investigate the macroscopic mechanical properties of granite samples, sampling was conducted from the III-level surrounding rock section of Lushi Dagangshan Tunnel. Considering the discrete nature of granite mineral composition, a set of rock samples was collected every 20 m along the longitudinal axis of the tunnel, resulting in a total of three sets. These samples were then processed into cylindrical standard specimens measuring 50 mm × 100 mm. The granite samples met the requirements specified in "Standard for Test Methods of Engineering Rock Mass" (GB/T 50266-2013), with end surface unevenness less than 0.05 mm and height error controlled within 0.3 mm, the finished specimen is shown in Figure 2A.

The mechanical properties of granite were evaluated using the TAW-1000D multi-function testing machine for rheological

FIGURE 1
Geological profile and sampling position.

FIGURE 2
Uniaxial compression test of granite.
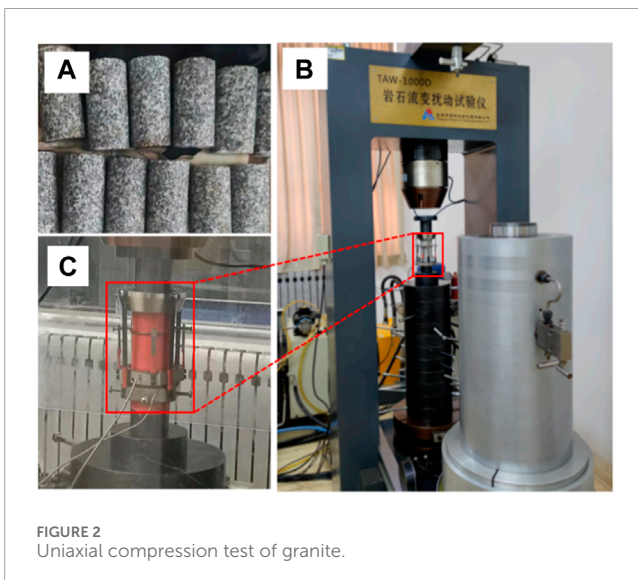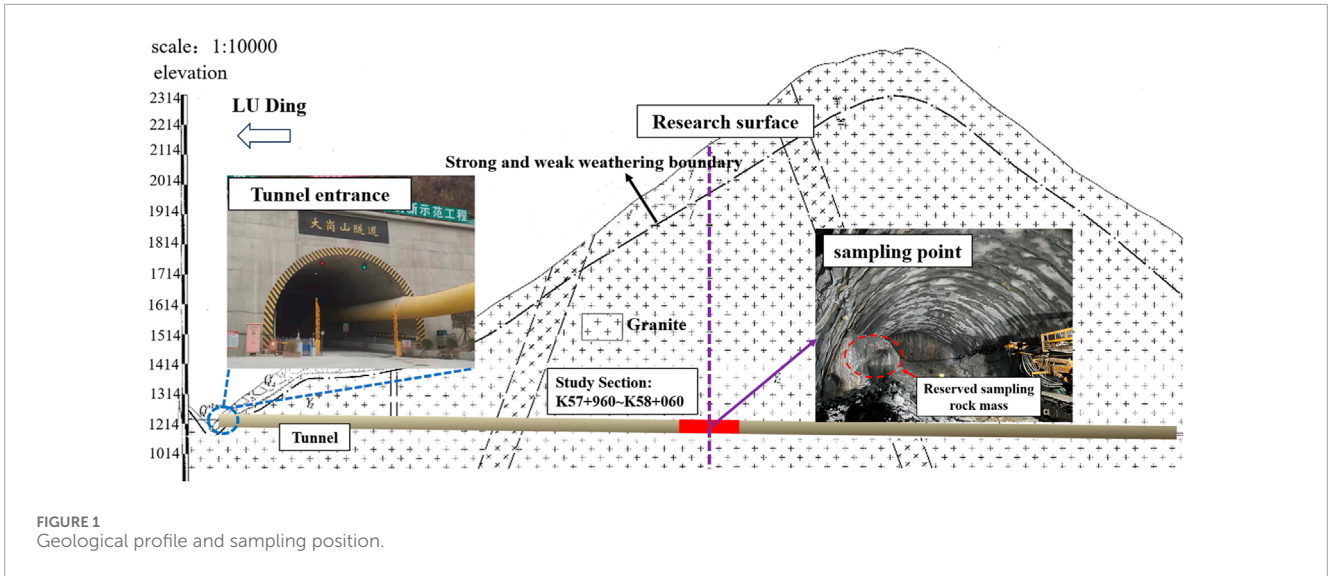
analysis of rock in the laboratory of rock mechanics at Shandong Jianzhu University. The maximum axial pressure capacity of the testing machine was 1,000 kN. At the onset of the test, the contact distance between the loading end and the top position of the specimen was initially increased at a rate of 20 mm/s. Once this contact distance reached approximately 1–2 mm, force control was implemented with a speed of 10 N/s. Subsequently, after complete contact between the testing machine and specimen was established, displacement control was switched to a loading rate of 0.1 mm/min. The experimental setup for conducting these tests is illustrated in Figure 2B, the placement of rock specimens is shown in Figure 2C, while Figure 3A presents the failure modes observed in each specimen tested. The entire test process data were recorded using axial strain gauges and a loading

system, with stress-strain monitoring curves depicted in Figure 3B (Chen et al., 2023).

The fracture morphologies of the three groups of rock samples are observed to be similar, as depicted in Figure 3. In the III-level surrounding rock section, compression predominantly damages the granite, while shear cracks originate from tensile stress during penetration. The angle between the tensile cracks and the main fracture surface is less than 90°, indicating that shear failure is primary with supplementary tensile failure. Macroscopic fracture analysis reveals a relatively smooth main fracture surface with adhering flocculent crystal particles. Additionally, micro-rock bursts occur during axial compression damage due to continuous loading, where released tensile stress leads to local rock caving and audible sounds.

According to the complete stress-strain curve, during the initial compaction stage (OA), the stress-strain relationship exhibits an uneven quadratic growth pattern. In the stage of elastic deformation (AB), the growth of the curve follows a linear function. The overall stability of the specimen in the initial two stages is excellent, with no occurrence of cracks within the area and no visible cracks on the rock surface. In the unstable fracture stage (BC), microcracks are initiated on the surface of the specimen, which subsequently propagate under increasing axial load. Localized detachment of rock fragments occurs, accompanied by acoustic emissions, indicating progressive development and expansion of internal cracks within the rock sample. The rate of stress growth gradually diminishes. Finally, in the overall failure stage (CD), peak stress is reached accompanied by a distinct "excessive noise," resulting in a rapid decline of the stress curve and formation of macro fractures as internal and external cracks connect. These findings indicate that granite within this III-level surrounding rock section possesses hard brittleness and high compressive strength. The process of crack initiation, propagation, and ultimate fracture within the rock mass involves energy migration with large-scale release upon loss of bearing capacity.
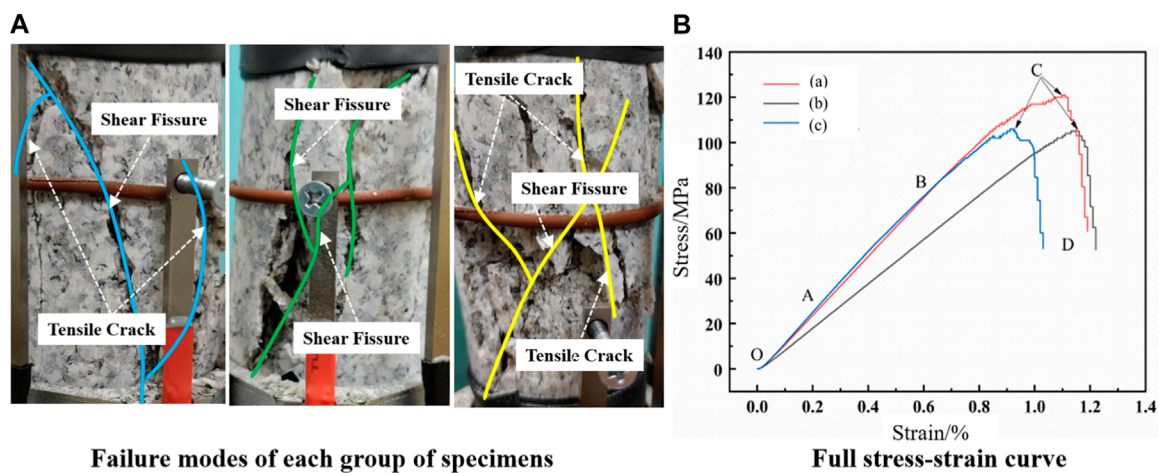
FIGURE 3
Rock failure mode and stress-strain curve.

4 Revealing the mineral composition and fracture behavior of granite via XRD analysis

4.1 XRD analysis of Granite's mineral composition

In order to investigate the influence of granite mineral composition on the fracture morphology and strength of rock mass, samples were randomly collected from three groups of indoor test specimens. The sampling location is illustrated in Figure 5, with a sampling size of 5 mm × 5 mm × 5 mm. After sampling, the granite samples should be ground uniformly in a dry environment free from any impurities. Once each group of granite powder has been ground to meet the standard specifications, all powders from these three groups should be combined and thoroughly mixed and ground together. The negative pressure test screen size should be Ø150 × 25. Finally, powder particles with a diameter less than 0.08 mm were extracted for mineral composition analysis using an X-ray diffraction instrument (XRD testing machine). Considering that the granite test blocks were obtained from the same batch of rock mass, it was assumed that their mineral composition content represented that of the engineering section and aligned with the microscopic properties of granite. The experimental procedure is depicted in Figure 4.

The XRD testing machine of Shandong Jianzhu University was utilized for the experiment, with an X-ray scanning range from 0° to 90°. Due to the unique crystal structure possessed by each mineral component, which acts as a three-dimensional grating for X-ray diffraction, when passing through this crystal structure, X-rays generate diffraction patterns with varying intensities. By analyzing the position and intensity of these diffraction lines in the patterns, it is possible to determine both the mineral composition and structure accurately. This principle of diffraction adheres to the Bragg formula, as shown in Formula 1.
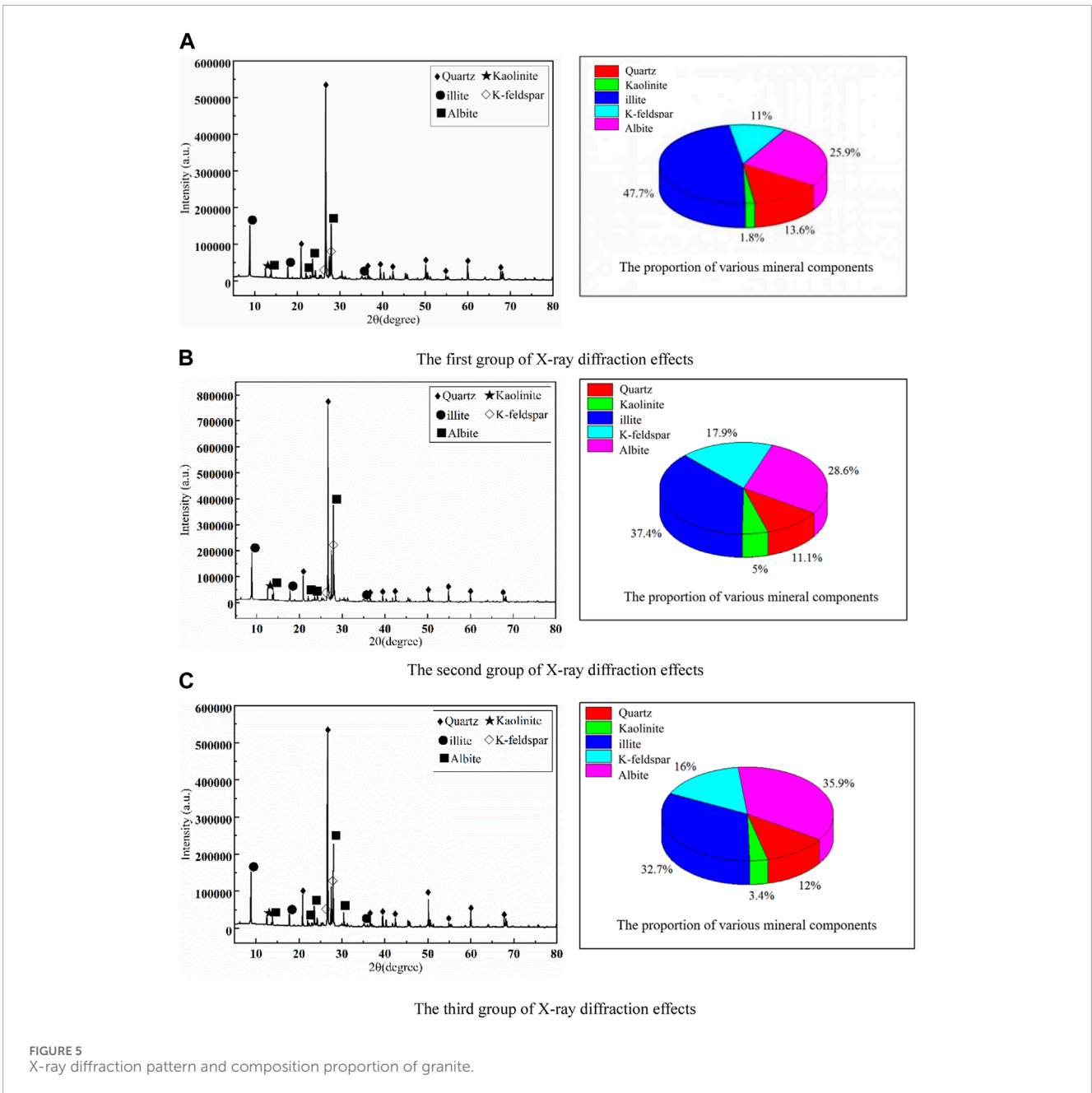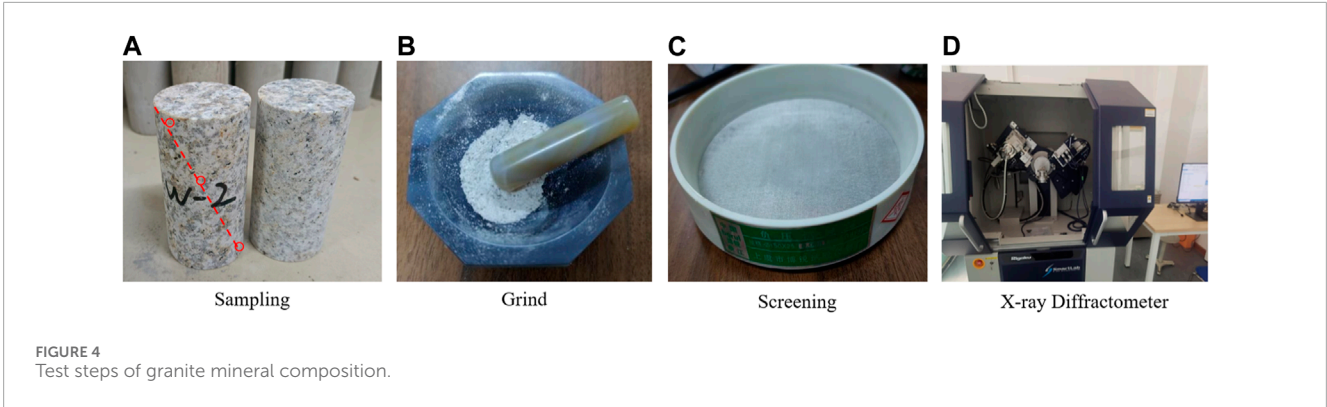
$$2d \sin \theta = n\lambda \qquad (1)$$

where d represents the interatomic spacing in the crystal, θ represents the half-diffractive angle, n represents the diffraction series, and λ represents the wavelength of X-ray radiation.

Following X-ray diffraction analysis on three groups of specimens, minerals corresponding to each peak value were identified and labeled in Figure 5. The respective RIR values for each mineral were obtained. The ratio of each mineral's RIR value to its modified diffraction intensity represented the adjusted intensity of that mineral, while the ratio of each mineral's adjusted intensity to the total diffraction intensity indicated its relative content. The X-ray diffraction patterns for each group and quantitative analysis results regarding granite mineral composition are presented in Figure 6.

The mineral composition of granite in the III-level surrounding rock section of Dagangshan is predominantly composed of illite $[Al_4Si_2O_9(OH)_3]$, albite ($NaAlSi_3O_8$), K-feldspar ($KAlSi_3O_8$), quartz (SiO_2), and kaolinite $[Al_4(OH)_8Si_4O_{10}]$, as depicted in Figure 5. Illite and albite exhibit the highest abundance with respective proportions of 39.3% and 30% among all minerals present. Conversely, kaolinite exhibits the lowest content. From the perspective of mineral hardness, quartz and feldspar minerals have significantly higher mineral strength than the other three, which are 7 and 6, respectively, while the hardness of illite is about 1–2, and the hardness of kaolinite is 2–2.5. According to Liu et al. (2019) study of granite and marble, it is found that mineral particles with weak hardness are more prone to fracture mechanical behavior under external load. Based on the strength and mineral content of these five minerals, the micro-fracture morphology and rock strength changes of mineral particles in inhomogeneous granite will be studied below.

4.2 SEM analysis of granite micro-fractures

The damaged rock mass after uniaxial compression is analyzed using scanning electron microscopy (SEM) technology. SEM can magnify the rock mass up to 100,000 times with a resolution reaching the nanometer level. By utilizing a focused electron
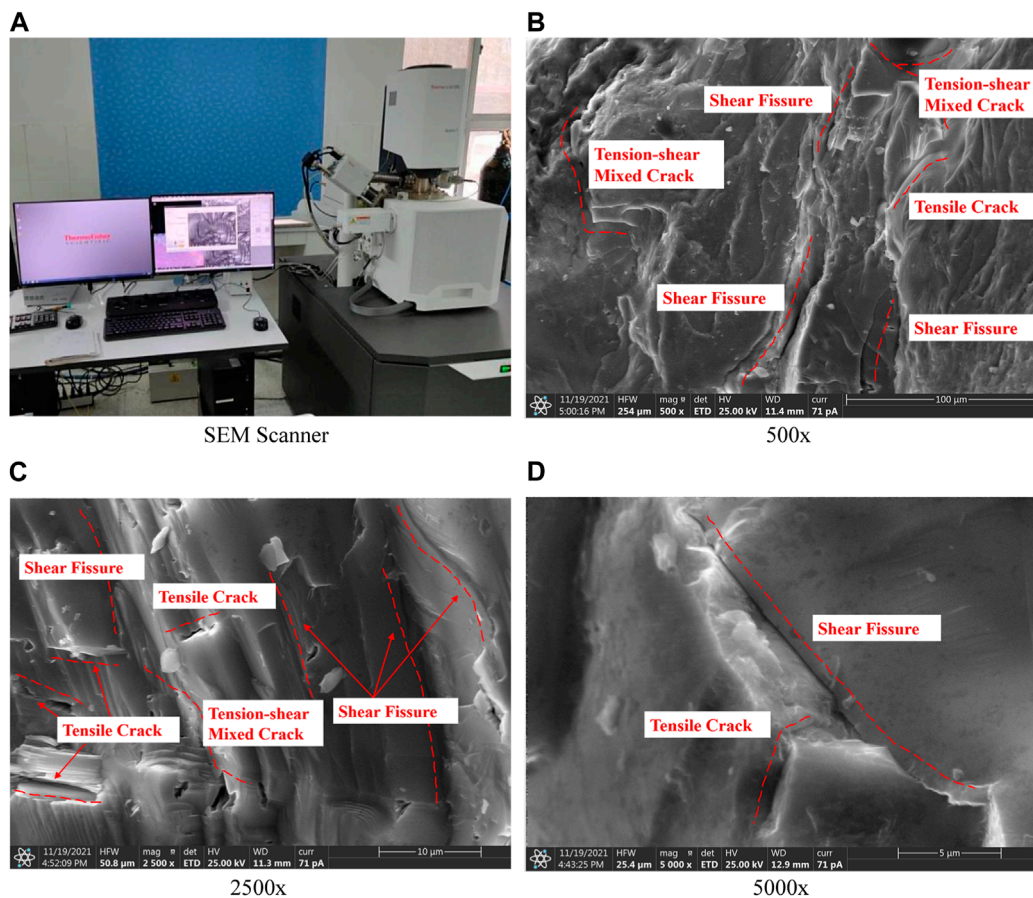
FIGURE 4
Test steps of granite mineral composition.

FIGURE 5
X-ray diffraction pattern and composition proportion of granite.

FIGURE 6
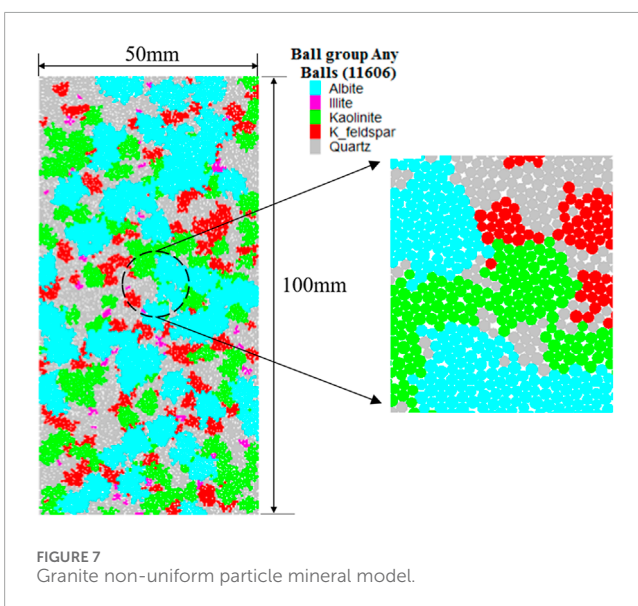SEM scanner and some test results of granite.

FIGURE 7
Granite non-uniform particle mineral model.

beam, SEM bombards the sample surface to generate secondary electrons, backscattered electrons, absorbed electrons, characteristic X-rays, and other physical signals. These signals are then captured, magnified, processed using various types of detectors and scanned point by point on the sample surface through a scanning coil for imaging purposes. Narrow focus high-energy electron beam scanning of specimens allows for interaction between the emitted beam and the sample material to represent its physical information behavior accurately. This process involves collecting, amplifying and re-imagining information in order to obtain microscopic morphological images of the samples.

The representative fracture section of granite was selected for laboratory testing, and subsequent SEM scanning analysis was conducted to examine its microscopic failure characteristics. The Thermo Scientific Quattro SEM system at Shandong University was employed for the SEM scanning. Prior to the experiment, ultrasonic cleaning was conducted on the samples to eliminate surface impurities. Subsequently, the granite fracture sections were scanned and analyzed under seven conditions: ×500, ×1,000, ×1,500, ×2,000, ×2,500, ×3,500, and ×5,000 magnifications. Figure 6 presents both the testing instrument used and some test results.

As depicted in Figure 6, the failure modes among particles exhibit three primary forms: shear fracture, tensile fracture, and tensile-shear composite fracture. Shear fracture plays a dominant role while tensile fracture and tensile-shear composite fractures act as auxiliary factors, which is consistent with the macroscopic characteristics of rock mass fracturing. Shear fractures are darker in

**TABLE 1** Physical and mechanical parameters of granite particle model.

Mineral names	Minerals proportion /%	Density ρ/(kg·m^{-3})	Effective Shot Sex modulus E_c/GPa	Stiffness ratio k_n/k_s	Rub coefficient mu	Porosity *Lambda.*	Tensile intensity σ_c/MPa	Cohesive force c/MPa	Friction angle Phi/(°)
Quartz	12.3	2,900	60	2.5	0.5	3e-5	265	280	35
Potash Feldspar	15.0	2,700	45	2.5	0.5	3e-5	130	135	30
Albite	30.1	2,650	42	2.5	0.5	3e-5	110	120	30
Illite	39.2	2,800	11	2.5	0.5	3e-5	30	50	27
Kaolin	3.40	2,850	18	2.5	0.5	3e-5	25	40	27

color, closer together and denser in closure, with longer elongation lengths that mainly occur along mineral particle slips. The meso-shear fractures of granite present a layered structure formed primarily by axial external force compression and natural joints along the granite crystal. Furthermore, based on our analysis of mineral particle hardness above, illite is identified as the weak mineral within the granite sample; thus generating obvious layered structural cracks on its surface during fracturing processes. These cracks develop over long distances with joint step surfaces parallel to them; this type of failure mode is more sensitive to external loads but requires less energy for internal fracturing.

The fracture with lighter color, larger width and shorter extension length is tensile fracture, which is mainly formed under tension. Tensile fracture mostly occurs between relatively complete quartz mineral particles. Due to the high strength and hardness of quartz minerals and the smooth jointless surface, the particles around the tensile fracture are irregularly concave and convex. The reason is that the crystal particles are brittle due to the action of tensile stress, and the crisp loud noise in the process of uniaxial compression test is mainly the fracture of quartz brittle mineral materials. There is also a local tensile-shear composite fracture between the two failures, and the fracture is mostly manifested as a twisted shape in the direction of tensile stress.

5 The correlation between macro-micro of granite and stability analysis of tunnel surrounding rock

Considering the analysis of tunnel surrounding rock stability, the utilization of finite element or finite difference analysis methods enables the simulation of macroscopic information such as surrounding rock stress and strain, thereby offering guidance for engineering construction. However, there is a lack of microscopic-scale research and an inability to establish a correlation between microscopic and macroscopic scales. Therefore, by employing XRD component analysis and SEM electron microscope scanning analysis in conjunction with laboratory test results, we utilize PFC software to construct a particle flow tunnel model and investigate the

FIGURE 8
Comparison of PFC particle flow simulation and laboratory test (Chen, et al., 2023)
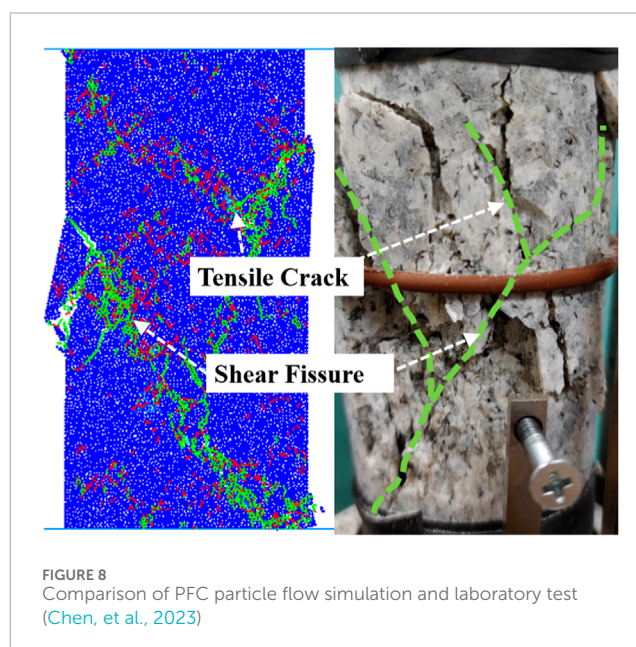
influence of microscopic components on the macroscopic failure of surrounding rock mass.

5.1 Construction and calibration of non-uniformity discrete element model

According to the requirements specified in the Standard for Test Methods of Engineering Rock Mass (GB/T50266-2013), a granite particle model is constructed with a diameter of 50 mm and a height ranging from 2.0 to 2.5 times the diameter (i.e., a height of 100 mm) using a linear parallel bonding model. The weak mineral illite is used as the reference point of PFC micro-adjustment parameters. According to the field survey report, the coefficients of particle porosity and particle radius range are assigned, and the equilibrium state is achieved by eliminating the "overlap cloud" between particles. Corresponding to the mineral composition of the XRD test, the ball group command was used to group the particles,
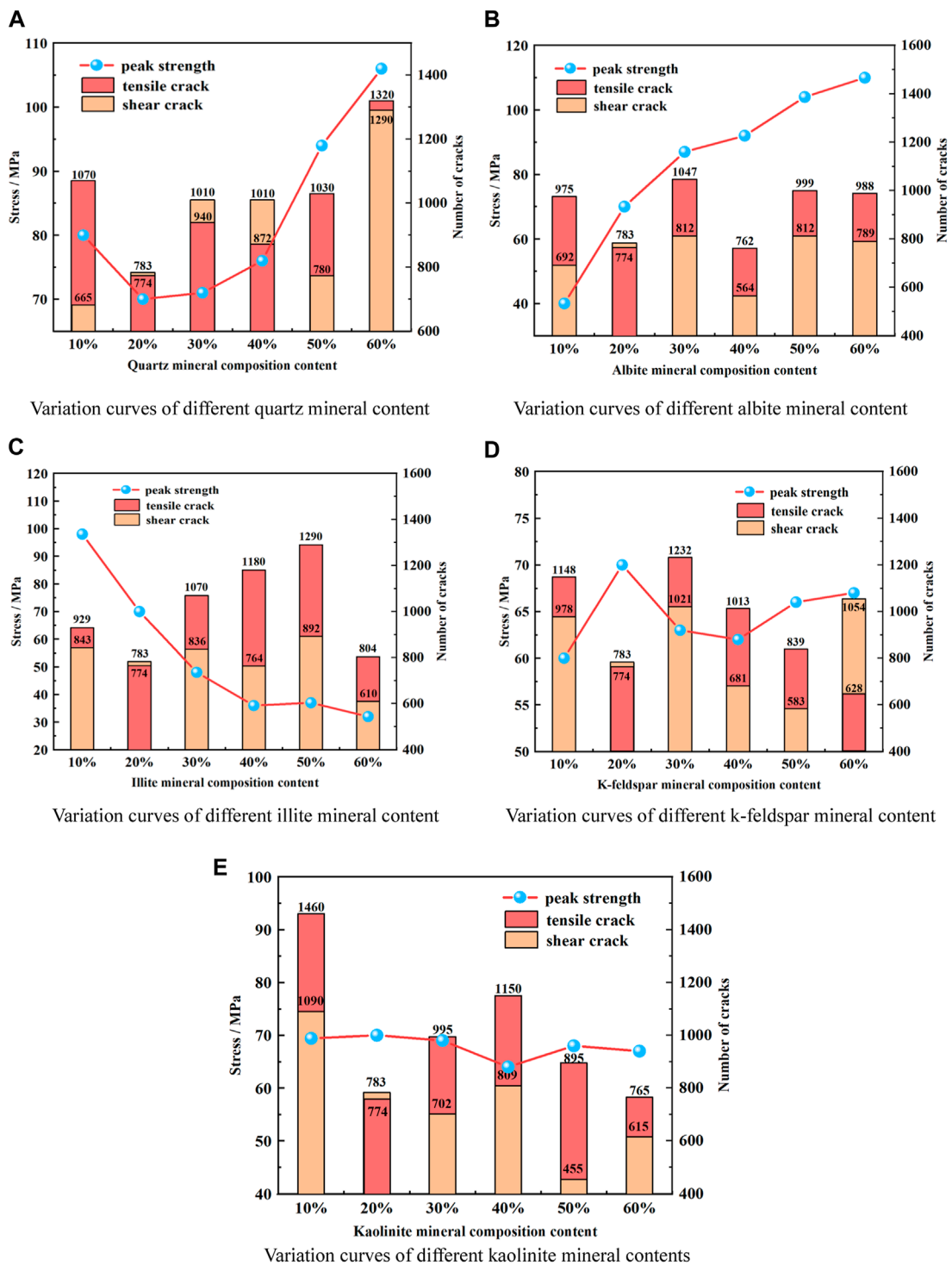
FIGURE 9
The curve of peak strength and failure crack of each mineral.

and the area ratio was used to control the random distribution of the mineral particles. The cluster particle family property of FISH language is developed to generate discrete element particles, and the distribution morphology of the grouped mineral particles is controlled according to the Weibull random distribution function. The distribution morphology, composition content and mineral

category conditions of specific minerals are controlled, and the generated non-uniform model particles are shown in Figure 7.

In this study, the parameters of the parallel bonding model were calibrated. Firstly, the elastic modulus was calibrated using direct tensile testing. Subsequently, the stiffness ratio coefficient (kratio) was determined through hypothesis analysis and mechanical testing.
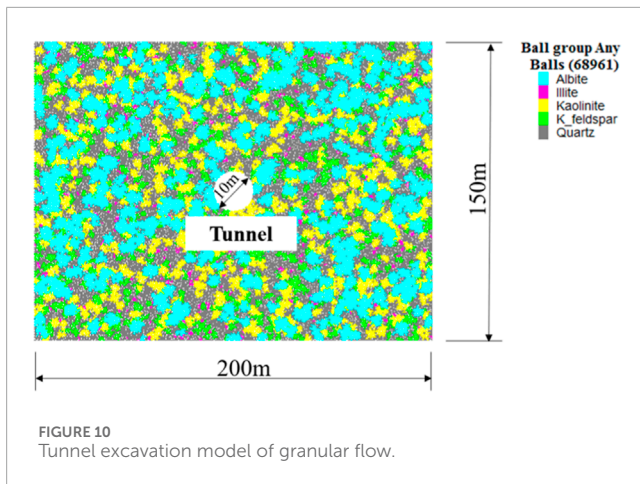
FIGURE 10
Tunnel excavation model of granular flow.

The range of bonding ratio was approximated based on failure mode and post-peak stress curve obtained from uniaxial compression tests on granite specimens, which ranged between 1.0 and 2.0 in our simulation. Finally, the peak strength served as a reference point for comparison with laboratory test results, ensuring that differences in peak strength remained within 5%.

By iteratively fine-tuning microscopic parameters based on calibration and mechanical properties derived from laboratory compression tests on granite particles, we established a set of parameters presented in Table 1. Using these parameters as a basis, we conducted simulations to compare against laboratory test results discussed earlier in this paper; Figure 8 illustrates the comparison outcomes.

The numerical simulation in Figure 8 reveals that, the numerical simulation results exhibit a high level of agreement with laboratory tests, displaying distinct "Y" type shear cracks along with some accompanying tensile cracks. Shear failure remains dominant in the final failure mechanism of the rock mass, albeit accompanied by tension. These calibrated parameters are believed to accurately reflect the mechanical behavior of grade III granite surrounding rock segment discussed in this paper. Consequently, based on this model, an analysis is conducted below to investigate how changes in microscopic parameters influence surrounding rock stability.

5.2 Relevance of microscopic composition alteration to macroscopic fracture

Based on the aforementioned non-uniform granite model, the influence of microscopic composition changes on macroscopic fracture in granite was further investigated by adjusting the proportion of each mineral content using the control variable method. Each mineral content was quantitatively increased or decreased by 10% individually, with a maximum mineral content of 60%. The remaining mineral content was equally distributed, accounting for approximately 10%, to avoid limitations imposed by insufficient mineral content on the non-uniformity granite model. The curve of crack number, stress change and peak strength changing with content under each working condition is shown in Figure 9.

As can be seen from Figure 9A, when the quartz content is within the range of 10%~20%, the failure of granite is mainly tensile cracks, which is consistent with the SEM test results. When the quartz content increases, the cracks turn to be mainly shear cracks. When the quartz content is high, tensile cracks play a dominant role. The increase in quartz content simultaneously enhances the overall strength of the rock, referred to as "enhanced minerals." As depicted in Figure 9B, the peak strength of albite also exhibits a linear increase with a significant magnitude, indicating that albite is also an "enhanced mineral" and effectively improves the rock's strength. The number of tensile cracks during overall failure is substantial, while the disparity between shear crack numbers remains relatively stable. As depicted in Figure 9C, the overall strength of rocks decreases with an increase in illite content, which is classified as a "weakened mineral." This suggests that illite is a weak mineral particle with poor bonding performance, and its internal particles are prone to breakage and damage due to slip, which is a contributing factor to weakened rock strength. This phenomenon also confirms the accuracy of SEM scanning tests in identifying illite as a weak mineral. Furthermore, Figures 9D, E demonstrate that an increase in K-feldspar and kaolinite mineral content does not significantly affect the peak strength or number of cracks in rocks; instead, it results in balanced mineral particles where tension cracks outnumber shear cracks.

5.3 Stability analysis of surrounding rock of Dagangshan tunnel

The composition of grade III surrounding rock in the section of K57+960~K58+060 of Dagangshan Tunnel has been determined through XRD testing, and the proportion represents the average value obtained from three sets of tests as shown in Figure 5. The physical and mechanical parameters are presented in Table 1. Considering the characteristics of PFC, this study adopts an equivalent cross-section area method to represent the tricentric tunnel section as a circular one with a diameter of 10 m. After accounting for boundary effects, the overall size of the model is set to be 200 m × 150 m, ensuring that there is a distance equal to five times the tunnel diameter between one side of the tunnel and the model boundary. A total number of 68,961 particles are generated within this calculation model, as illustrated in Figure 10. The fracture patterns exhibited by mineral particles within surrounding rock after tunnel excavation and collapse disasters occurring in field sections are depicted in Figure 11.

According to the numerical simulation analysis in Figure 11A, the tunnel displacement field distribution of the non-uniform granite numerical model is basically consistent with the conventional modeling law, indicating that the application of non-uniformity modeling method is accurate. Blue represents albite, and gray represents quartz. Albite is mainly destroyed by shearing through mineral particles, and a small amount of rock burst particles are scattered on the edge of the tunnel, which are mainly sheared minerals of albite. It can be seen from the surrounding rock near the tunnel entrance that the quartz mineral structure basically has no cracks, and a small part of surrounding rock particles are destroyed by quartz sliding along mineral particles, indicating that the expansion and penetration of cracks around the "enhanced
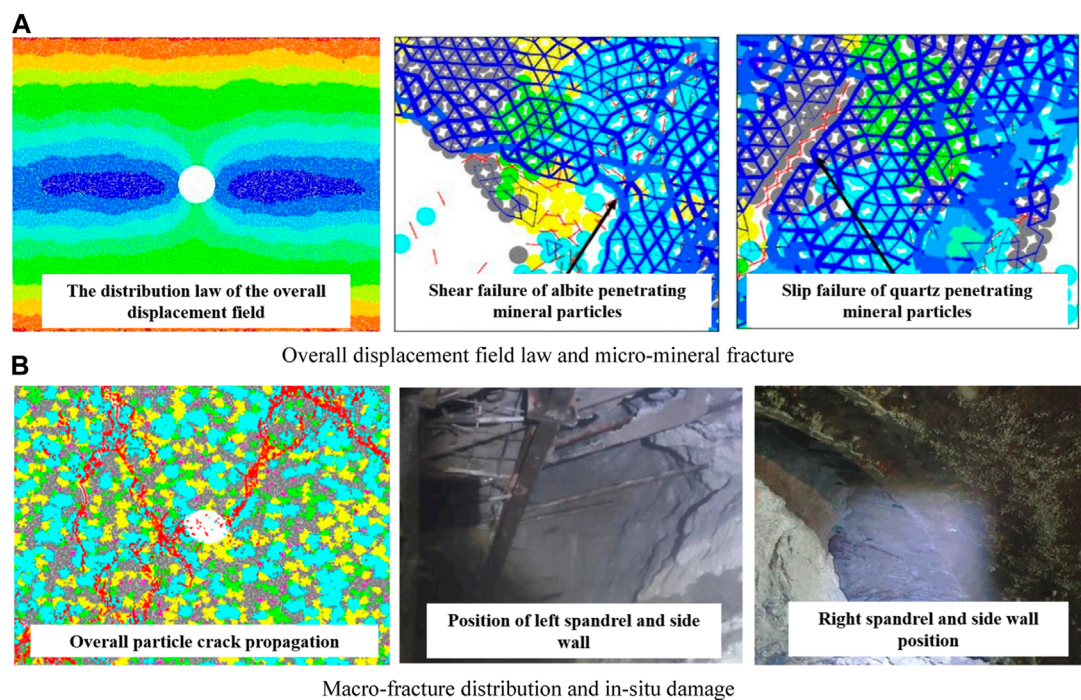
FIGURE 11
Fracture pattern of surrounding rock in tunnel excavation.

minerals" are not obvious. As can be seen from Figure 11B, three obvious shear fracture zones appear in the surrounding rock of the tunnel excavation, mainly caused by the expansion and penetration of cracks in the purple mineral, namely, illite area, indicating that the strength of the "weakened mineral" itself and the force chain strength between minerals are far lower than that of the "enhanced mineral." Therefore, the content and distribution of the "weakened mineral" have a greater impact on the stability of the surrounding rock. The left and right arch shoulders and side walls are damaged seriously during tunnel excavation, and the main damage is shear fracture. Figure 11B shows the rock mass collapses of the left and right arch shoulders and the upper side walls after the chain disaster occurs in the tunnel, which are in good agreement with the numerical simulation results. Therefore, it is suggested to strengthen the support measures of the left and right arch shoulders and side walls under similar working conditions.

6 Conclusion

(1) Shear fracture is the predominant mode of failure in grade III granite under compression. The primary fracture surface exhibits a smooth texture, with flocculent crystal particles adhering to it. Additionally, tension cracks are observed surrounding the main fracture surface. The rock mass demonstrates evident hardness and brittleness, resulting in a pronounced release of instantaneous energy upon loss of bearing capacity, producing a crisp sound.

(2) XRD analysis can better determine the composition and proportion of rock minerals. Combined with SEM electron microscope scanning, the microscopic angle shows that the fracture of rock fracture plays a controlling role, supplemented by tensile fracture and tensile-shear composite fracture, and the fracture mainly occurs in the enrichment area of weak minerals such as illite.

(3) Among the minerals in the granite, quartz and albite are "enhanced minerals," which are mainly characterized by the increase of rock strength with the increase of content, while illite is "weakened minerals." The stability of the surrounding rock in tunnels is primarily influenced by the presence of "weakened minerals," whereas "enhanced minerals" tend to exhibit inherent stability due to their hardness and strong inter-mineral bonding. Following tunnel excavation, the most severe issues arise from cracking observed in both left and right arch shoulders as well as side walls; therefore, it is imperative to reinforce the supporting function of this particular section.

Data availability statement

The original contributions presented in the study are included in the article/supplementary material, further inquiries can be directed to the corresponding author.

Author contributions

YC: Data curation, Funding acquisition, Methodology, Writing–review and editing, Writing–original draft. JS: Data curation, Writing–original draft. TG: Methodology, Software,

Writing–original draft. YJ: Writing–review and editing, Resources, Software. HZ: Writing–review and editing. HD: Writing–review and editing. WZ: Writing–review and editing.

Conflict of interest

The authors declare that the research was conducted in the absence of any commercial or financial relationships that could be construed as a potential conflict of interest.

Publisher's note

All claims expressed in this article are solely those of the authors and do not necessarily represent those of their affiliated organizations, or those of the publisher, the editors and the reviewers. Any product that may be evaluated in this article, or claim that may be made by its manufacturer, is not guaranteed or endorsed by the publisher.

References

Chen, X., Zhou, X., Xu, B., et al. (2022b). Investigation on the macro-micro shear damage mechanical behaviors of fractured rocks. *Chin. J. Rock Mech. Eng.* 41, 0–10. doi:10.13722/j.cnki.jrme.2022.0152

Chen, Y., Gao, T., Gao, C., et al. (2022a). Fracture propagation and acoustic emission energy damage law of fractured rock mass under hydraulic coupling action. *J. Central South Univ. Sci. Technol.* 53 (6), 2325–2335. doi:10.11817/j.issn.1672-7207.2022.06.032

Chen, Y., Gao, T., Yin, F., Liu, X., and Wang, J. (2022c). Study on influence of joint locations and hydraulic coupling actions on rock masses' failure process. *Energies* 15 (11), 4024. doi:10.3390/en15114024

Chen, Y., Liu, M., Gao, T., and Jing, Y. (2023). Macro–micro failure and energy evolution in heterogeneous fault rock masses. *Geotechnical Geol. Eng.*, 1–15. doi:10.1007/s10706-023-02705-0

Gao, T. (2022). *Study on macroscopic and microscopic failure and energy evolution of inhomogeneous granites*. Jinan: Shandong Jianzhu University. doi:10.27273/d.cnki.gsajc.2022.000589

Han, J., Wang, J., Yang, W., Wang, X., Ma, R., Wang, W., et al. (2023). Experimental study on the properties of a polymer-modified superfine cementitious composite material for waterproofing and plugging. *Case Stud. Constr. Mater.* 19, e02552. doi:10.1016/j.cscm.2023.e02552

Huang, N., Jiang, Y., Cheng, Y., et al. (2021a). Experimental and numerical study of hydraulic properties of three-dimensional rough fracture networks based on 3D printing technology. *Rock Soil Mech.* 42 (6), 1659–1680. doi:10.16285/j.rsm.2020.1448

Huang, X., Xiao, P., Dong, L., et al. (2021b). Mechanical response and failure mechanism of rock mass during excavation of underground caverns under high geostress. *Hazard Control Tunn. Undergr. Eng.* 3 (3), 85–93. doi:10.19952/j.cnki.2096-5052.2021.03.09

Li, H. (2017). *Aging rupture mechanism and microscopic evolution mechanism of deep heterogeneous rock mass*. Wuhan: Changjiang River Scientific Research Institute.

Li, T., Zhao, W., Liu, R., Han, J., Jia, P., and Cheng, C. (2023). Visualized direct shear test of the interface between gravelly sand and concrete pipe. *Can. Geotechnical J.* 61, 361–374. doi:10.1139/cgj-2022-0007

Liu, W., Lu, Q., Guo, S., et al. (2021). Study on the hydro-mechanical coupling numerical model for layered rocks based on macro-micro structures. *Chin. J. Rock Mech. Eng.* 40 (Suppl. 1), 2851–2860. doi:10.13722/j.cnki.jrme.2020.0789

Liu, X., Liu, Z., Li, X., et al. (2019). Acoustic emission and micro-fracture characteristics of rock under splitting load. *J. Eng. Sci.* 41 (11), 1422–1432. doi:10.13374/j.issn2095-9389.2018.11.29.005

Liu, Z., Zhang, L., Liu, G., Li, W., Li, S., Wang, F., et al. (2020). Material constituents and mechanical properties and macro-micro-failure modes of tight gas reservoirs. *Energy Explor. Exploitation* 38 (6), 2631–2648. doi:10.1177/0144598720913069

Ni, H., Xu, W., Shi, A., et al. (2015). Scale effect on equivalent continuum elastic modulus of columnar jointed rock masses by distinct element method. *Eng. Mech.* 32 (3), 90–96. doi:10.6052/j.issn.1000-4750.2013.09.0849

Peng, Z., Zeng, Y., Chen, X., and Cheng, S. (2021). A macro-micro damage model for rock under compression loading. *Appl. Sciences-Basel* 11 (24), 12154. doi:10.3390/app112412154

Shi, X., Guan, Q., Wang, W., et al. (2020). Numerical simulation of rock fragmentation process by TBM cutter in double-joint rock mass. *J. Shandong Univ. Eng. Sci.* 50 (4), 70–79. doi:10.6040/j.issn.1672-3961.0.2019.744

Sun, H., Belhaj, H., Tao, G., Vega, S., and Liu, L. (2019). Rock properties evaluation for carbonate reservoir characterization with multi-scale digital rock images. *J. Petrloeum Sci. Eng.* 175, 654–664. doi:10.1016/j.petrol.2018.12.075

Tang, C., Liang, Z., Yang, T., et al. (2005). Three-dimensional damage soften model for failure process of heterogeneous rocks and associated numerical simulation. *Chin. J. Geotechnical Eng.* 27 (12), 1447–1452. doi:10.3321/j.issn:1000-4548.2005.12.015

Vahid, M., and Abbas, M. (2021). Directional rock mass rating (DRMR) for anisotropic rock mass characterization. *Bull. Eng. Geol. Environ.* 80 (6), 4471–4499. doi:10.1007/s10064-021-02143-3

Xia, Y., Meng, Q., Tang, C., et al. (2021). Applications of realistic failure process analysis in tunnel engineering disaster simulation. *Hazard Control Tunn. Undergr. Eng.* 3 (3), 36–49. doi:10.19952/j.cnki.2096-5052.2021.03.05

Xu, Z., Yu, S., and Fu, Q. (2020). Numerical simulation of mechanical properties of layered jointed rock mass. *J. Shandong Univ. Eng. Sci.* 50 (3), 66–72. doi:10.6040/j.issn.1672-3961.0.2019.393

Yang, Y. (2018). *Study on macroscopic and micro mechanical characteristics of coarse-grained Soil fillers based on triaxial and CT test*. Changsha: Changsha University of Science and Technology. doi:10.26985/d.cnki.gcsjc.2018.000327

Yang, Z., Ning, Y., Luo, M., et al. (2016). Characterization of rock heterogeneity modeled by discontinuous deformation analysis method. *J. Chongqing Univ.* 39 (5), 97–102. doi:10.11835/j.issn.1000-582X.2016.05.013

Zhang, K., Wang, L., Lu, Y., et al. (2017). Study on numerical simulation of rock under true triaxial stress. *Coal Technol.* 37 (4), 68–71. doi:10.13301/j.cnki.ct.2018.04.026

Zheng, L., He, H., Zou, Y., Liu, H., Liu, X., and Qiu, Q. (2022). Research on macro-micro failure mechanism of interbedded sandstone in the deep of lannigou gold mine. *Lithosphere* 2022, 2998830. special 10). doi:10.2113/2022/2998830

Zheng, X., Hu, Z., Liu, C., et al. (2005). Deformation characteristic of crack rock fatigue failure by using CT testing. *J. Xi'an Univ. Sci. Technol.* 25 (4), 469–472. doi:10.3969/j.issn.1672-9315.2005.04.015